Nano Energy 42 (2017) 300–306

Contents lists available at ScienceDirect

Nano Energy

journal homepage: www.elsevier.com/locate/nanoen

Full paper

Fully stretchable and highly durable triboelectric nanogenerators based on gold-nanosheet electrodes for self-powered human-motion detection

Guh-Hwan Lim[1], Sung Soo Kwak[1], Nayoung Kwon, Taekyung Kim, Han Kim, Seong Min Kim, Sang-Woo Kim[*], Byungkwon Lim[*]

School of Advanced Materials Science and Engineering, Sungkyunkwan University (SKKU), Suwon 16419, South Korea

ARTICLE INFO

Keywords:
Au nanosheet
Stretchable
Triboelectric nanogenerator
Motion detection
Self-powering

ABSTRACT

A patchable triboelectric nanogenerator (TENG) is highly promising for self-powered human-motion detection, but it may undergo repeated stretching/releasing cycles during daily activities of a human, which may lead to mechanical fracture of each component and degradation in electrical output performance of the TENG device. Here, we report a fully stretchable and durable triboelectric nanogenerator (TENG) with gold (Au) nanosheets (NSs) embedded into both PDMS matrix and micropyramid-patterned PDMS. It was found that a new design of the Au NS electrodes dramatically improves the mechanical flexibility and stretchability, enabling to achieve the outstanding output stability of the Au NS electrode-based TENG (Au NS-TENG) during 10,000 cycles of repeated pushing and stretching tests. Our fully stretchable and durable Au NS-TENGs were successfully applied to the hand joints that can be used in the self-powered human-motion detection processes for wearable applications.

1. Introduction

Recent interest in wearable or portable electronic devices has raised concerns about high-quality flexibility and stretchability, which are of interest to next-generation electronic device applications such as flexible displays, flexible and/or stretchable circuits, artificial electronic skins (e-skins), and various form-type sensors [1–6]. Accordingly, the need to replace or charge the battery must be removed regarding such electronic devices; otherwise, a heavier, separate power supply will remain a technological hurdle to user comfort over a long time period [7,8].

Recently, a new type of power-generation device called a triboelectric nanogenerator (TENG) has been developed based on the coupling mechanism between the triboelectric charge and the electrostatic induction for which mechanical energy, which is one of the most common energy sources in the surrounding environment, is used [9–12]. Because of the many advantages of the TENG, such as a low cost, a simple manufacturing process, and a high power density [13–18], the TENG can be successfully demonstrated without a battery or an external power supply due to the use of promising device and application energy-harvesting technologies such as voice-recognition devices, distress-signal emitters, trace-memory systems, velocity sensors, electroplating, electropolymerization, and water splitting [19–23]. In the TENGs, the triboelectric charging occurs at the contact interface through a periodic repetitive physical contact between two different materials of different polarities in terms of the triboelectric series, so the contact surface must be able to generate a robust and stable electrical output [24–26]. Although many TENGs have been previously reported, the reports of TENGs that are highly elastic, durable, and robust against repetitive external movements are rare.

To achieve devices that are 100% human-wearable, all of the components that make up the device must be flexible and stretchy [27–30]; particularly, the flexibility and stretchability of the electrode portion that serves to transfer the carrier to the external circuit to drive the device must be excellent [31–33]. However, most of the previously reported TENGs are lacking because the metals of the conductive electrodes in the TENGs such as gold (Au), aluminum (Al), or copper (Cu), which are not stretchable generally, are considered as the counterparts of triboelectric films [34–39].

To overcome this hurdle, it has become necessary to develop flexible and stretchable electrodes that are mechanically robust, electrically stable, and reliable for repetitive external forces. In this study, a fully stretchable and durable TENG is developed using Au nanosheet (NS)-embedded electrodes. The Au NS electrodes were built into the following two layers: the opposite side of the patterned polydimethylsiloxane (PDMS) for the top electrode and the friction layer (if it also serves as the bottom electrode). Also, the operating mechanism of the Au NS electrode-based TENG (Au NS-TENG) was confirmed in the

* Corresponding authors.
E-mail addresses: kimsw1@skku.edu (S.-W. Kim), blim@skku.edu (B. Lim).
[1] These authors contributed equally to this work.

https://doi.org/10.1016/j.nanoen.2017.11.001
Received 4 October 2017; Received in revised form 1 November 2017; Accepted 2 November 2017

pushing and stretching modes using the COMSOL software. The new design of Au NS electrodes dramatically improves the mechanical flexibility and stretchability, demonstrating the proposed TENG's outstanding output stability over 10,000 cycles of repeated pushing and stretching tests. Therefore, the proposed Au NS-TENG can be successfully applied to the hand joints that can be used in the self-powered human-motion detection processes for wearable applications.

2. Material and methods

2.1. Synthesis of the Au NS

According to the typical synthesis of Au NSs, 5 mL of aqueous solution containing 1.7 mg of L-arginine (Sigma Aldrich) was hosted in a 20-mL vial at room temperature and the solution was heated to 95 °C. Meanwhile, 2 mL of aqueous solution containing 13.5 mg of hydrogen tetrachloroaurate trihydrate ($HAuCl_4 \cdot 3H_2O$) that was obtained from Alfa Aesar was injected into the L-arginine solution using a pipette. The reaction mixture was maintained at 95 °C for 2 h and then cooled down to room temperature.

2.2. Fabrication of the Au NS-embedded electrodes

A Petri dish was filled with deionized water, and the Au NS dispersion in 1-butanol was dropped onto the water surface using a pipette. When the monolayer film of the Au NSs was formed at the water surface, the Au NS film was brought into contact or scooped up by an Si-wafer coated with a Teflon substrate. The multilayer Au NS film was obtained by repeating this process. Then, the Au NS film on the substrate was annealed at 100 °C for 10 min. The Sylgard 184 PDMS (Dow Corning) was prepared by mixing the base and the curing agent with a weight ratio of 10:1. The liquid PDMS was poured onto the Au NS film and then cured at 80 °C for 6 h. After the PDMS curing, the Au NS film-embedded PDMS matrix was peeled off from the glass substrate. Cu wires were connected to the Au NS film-embedded PDMS matrix using a silver paste, and the wire was coated with PDMS glue. The Au NS-embedded electrode with the micropyramid-patterned PDMS (100 μm in width) was fabricated using the same protocol; however, the micropyramid-patterned Si wafer was covered with the Au NS film/liquid PDMS on the Si-wafer substrate.

2.3. Characterization of the Au NS-embedded electrodes

Field emission scanning electron microscope (FE-SEM) images were captured using the SUPRA 55VP device (Carl Zeiss). Atomic force microscope (AFM) images were obtained using the XE100 device (PSIA) under tapping modes. The electrical performance of the Au NS electrode was measured using the Keithley 2634B device (Tektronix).

2.4. TENG measurements

All of the device measurements were performed under ambient conditions (temperature = 23 °C and relative humidity = 25–40%). A DPO 3052 digital phosphor oscilloscope (Tektronix) and the SR570 low-noise current preamplifier (Stanford Research Systems, Inc.) were used to measure the electrical properties of the TENG.

3. Results and discussion

Fig. 1a shows the schematic illustration of a highly stretchable and durable electrode based on a multilayered Au NS film-embedded PDMS matrix. The Au NSs that were used in this study were synthesized using the previously reported method, and the thickness and lateral size are 20 nm and 20–50 μm, respectively (Fig. S1) [6,40,41]. First, an Au NS multilayer film was prepared by transferring a monolayer of the Au NSs that were floating on a water surface onto a silicon (Si) wafer coated with polytetrafluoroethylene (PTFE) film followed by a repeating of the transfer process. After each transfer, the film was annealed at 100 °C for 10 min. Thermal annealing at this mild temperature increases the contact between stacked Au NSs. Then, the liquid PDMS was cast onto the Au NS film, which filled the spaces between the NSs. After the PDMS curing, the Au NS film-embedded PDMS matrix was detached from the substrate. The weak adhesion between the Au NS film-embedded PDMS matrix and the PTFE-coated substrate facilitated a clean

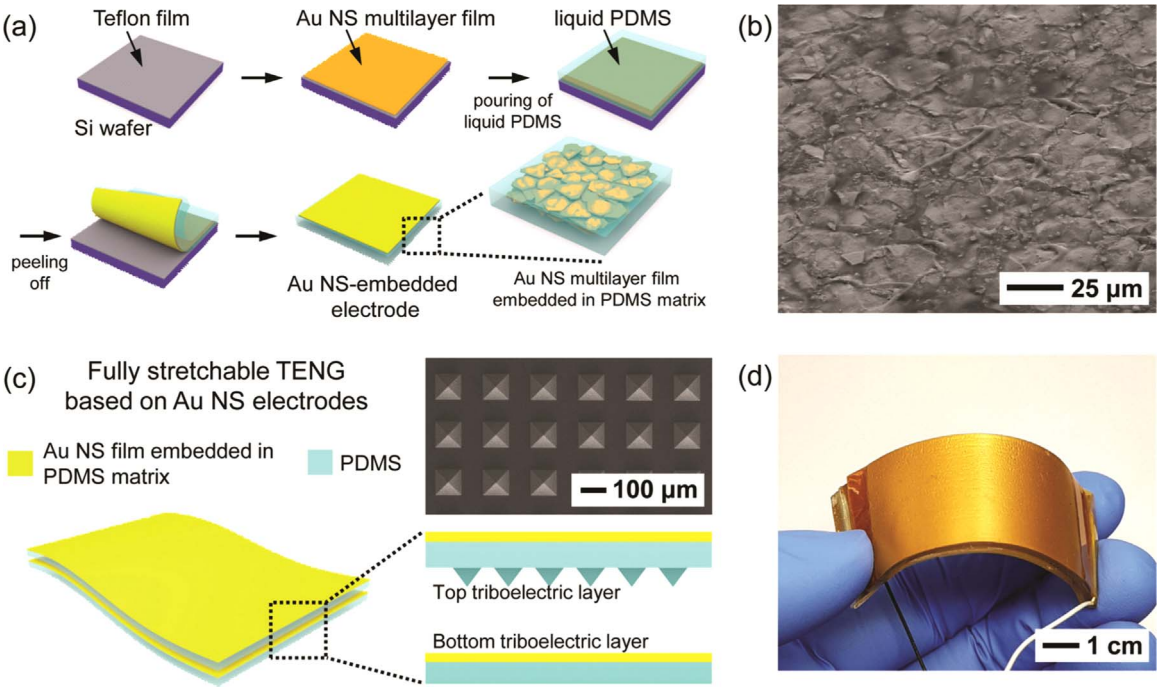

Fig. 1. (a) Schematic illustration of the fabrication process of the Au NS-embedded electrode. (b) Top-view FE-SEM image of the Au NS-embedded electrode. (c) Schematic illustration of the structure of the fully stretchable TENG based on the Au NS-embedded electrodes. The FE-SEM image shows the micropyramid-patterned PDMS (10 μm width) of the top triboelectric layer of the TENG. (d) Photograph of the Au NS-TENG.

delamination of the electrodes.

A field emission scanning electron microscopy (FE-SEM) analysis of the Au NS-embedded electrode revealed that the Au NSs were densely overlapped and partially embedded in the PDMS matrix (Fig. 1b). Fig. 1c shows the structural details of a fully stretchable and highly durable TENG that is based on the Au NS-embedded electrodes. This TENG consists of two Au NS-embedded electrodes, which are in contact with each other (Fig. 1c). The Au NS-embedded electrode of the top layer is micropyramid-patterned (100 μm-width) to increase the contact surface and the friction. Fig. S2 illustrates the fabrication process of the Au NS-embedded electrodes with the micropyramid pattern for its use as the top triboelectric layer of the TENG. The other Au NS-embedded electrode of the bottom layer serves as not only an electrode but also as friction material. The multilayered Au NS film is partially exposed on the surface of the NS-embedded PDMS electrode. Accordingly, the friction occurs between the micropyramid-patterned PDMS of the top layer and the Au NS film exposed on the surface of the bottom layer. Fig. 1d shows a photograph of an Au NS electrode based TENG (Au NS-TENG), the structure of which is very simple, wherein two Au NS films are embedded in the respective PDMS matrices of the top and bottom layers.

The mechanical robustness of the Au NS-embedded electrodes was investigated by monitoring the resistance change during the stretching- and detachment-cycle tests. Fig. S3 shows the electrical characteristics that are related to the number of Au NS layers in response to tensile strain. The electrical property of Au NS electrodes can be tuned by adjusting the number of Au NS layers that are transferred onto the substrate. When the multilayer Au NS film embedded in the PDMS matrix is stretched, the Au NSs can slide over one another, resulting in a change of the electrical resistance [6,40]. Since the area occupied by the Au NS layer becomes dense as the Au NS layer is increased, the resistance change (R/R_0) is decreased as the number of Au NS layers is increased during the stretching test. In this study, the Au NS-embedded electrodes prepared by the six-time transfer of the Au NSs for the TENG was used to obtain the electrical stability and reliability for the repetitive external strain.

For a comparison, a stretchable electrode that is based on an Au NS multilayer film was fabricated using the same protocol, with the exception of the Au NS multilayer film directly deposited onto the PDMS substrate. Both electrodes exhibited similar resistance-change behaviors due to a stretching up to a strain of ~ 30%, as shown in Fig. 2a. At larger strains (> 30%), the Au NS-embedded electrode exhibited a slightly larger R/R_0 than the Au NS on the PDMS electrode. The resistance of the Au NS-embedded electrode remained nearly unchanged during and after the 10,000 cycles of stretching at a tensile strain of 30%, as shown in Fig. 2b, thereby demonstrating its excellent electrical stability against repeated mechanical deformations. However, the Au NS on the PDMS electrode exhibited continuous and large resistance increases during the repeated stretching/releasing cycles at the same tensile strain.

The excellent electrical stability of the Au NS-embedded electrode could be explained by an interlocking of the Au NS into the PDMS matrix, which allows the Au NS film network to withstand an applied tensile strain to maintain the original percolating film network without a delamination during the stretching/releasing cycles (Fig. S4). However, the poor stability of the Au NS on the PDMS electrode could be explained by a poor adhesion of the Au NS onto the PDMS substrate, which leads to the delamination of the Au NS film percolating network that in turn rapidly increases the resistance (Fig. S5). The electromechanical stability of the Au NS-embedded PDMS electrodes is also superior to that of linear silver nanowire-embedded PDMS electrodes. In the latter, the linear nanowires are likely to undergo mechanical fracture during repeated tensile strains, which results in the disconnection of electrical paths and thus leads to continued increase in electrical resistance [42]. This Au NS-embedded electrode also exhibited a high stability against a Scotch-tape detachment test, with its resistance remaining constant during 100 detachment cycles; however, the resistance of the Au NS on the PDMS electrode dramatically increased over several detachment cycles (Fig. 2c). Fig. 2d shows the tape-contact regions of Au NS electrodes after the detachment test. These results suggest that the Au NS-embedded electrodes are suitable for fully stretchable and highly durable TENG applications.

When a stretchable Au NS-TENG is attached to the body, the two orientations of the input mechanical force are the vertical-push and horizontal-stretch directions. To describe these two work-mechanism cases, two independent work modes, as shown in Fig. 3, were simulated [14,43,44]. First, in the vertical motion, the micropyramid-patterned PDMS of the upper layer and the Au NS film embedded in the PDMS of the lower layer were periodically separated from each other and charged with the opposite signs (+Q & −Q) using triboelectrification. In addition, the surface of the patterned PDMS was altered by a plasma treatment in a tetrafluoromethane (CF_4) gas atmosphere to change the functional groups for the further increasing of the triboelectric surface charge at the contact interface [45–47].

When the Au NS-TENG was released, a potential difference between the upper electrode and the lower electrode became evident due to an electrostatic induction. To achieve equilibrium, the electrons flow from the top electrode to the bottom electrode through an external circuit, followed by their movement back to the top upon the approach of the two layers, as shown in Fig. 3a. The resultant electrical signal also depends on the contact area between the micropyramid-patterned PDMS and the Au NS, as the pyramidal pattern is modified so that it can be planarized by the application of a pushing force [25,48,49]. To provide a more detailed explanation, when the gap distance and the contact area were changed by the external pressing force, the COMSOL-software finite element method was employed after the measurement of the surface-charge density for which Eq. (1) was used with atomic force microscopy (AFM), and the potential distribution in the open-circuit condition was simulated, as shown in Fig. 3b. The potential distribution of the open-circuit voltage (V_{oc}) is defined as follows [50,51]:

$$V_{OC} = \frac{\sigma \cdot x}{\varepsilon_0} \tag{1}$$

where σ is the surface-charge density, x is the gap distance between the top and bottom electrodes, and ε_0 is the vacuum permittivity. The electrical potential between the two electrodes is reduced as the gap distance is decreased but the contact area is increased [52].

Second, the upper and lower layers with the opposite triboelectric charges in the initial state of the horizontal stretching motion are in contact with each other without a deformation of the micropyramid-patterned PDMS. When the Au NS-TENG was stretched, the height of each pyramid was decreased as the width of the pyramid was expanded, preserving the entire volume of the pyramidal structure with a slightly increased contact area, depending on the elongation degree. As with the workings of vertical motion, the alternating electrical signal was generated by the electron flow through the circuit during the periodic stretching and releasing, as shown in Fig. 3c. The potential distributions that vary with the strength of the stretching strain were also simulated using the COMSOL software, as shown in Fig. 3d.

The output performance of the Au NS-TENG with the dimensions of $2 \times 2\ cm^2$ was evaluated according to the repeated pushing and stretching cycles through the linear motors with vertical and parallel movements (Fig. 4). The Au NS-TENG exhibited excellent electrical output stability against a large number of repeated pushing/releasing cycles. The maximum-output voltage (which is measured with a load resistance of 40 MΩ) and current (which is measured with a load resistance of 100 Ω) were increased from 39.4 to 98.9 V and from 0.9 to 2.8 μA, respectively, by an increasing of the pushing force from 1 to 6 N because the contact area between the patterned pyramidal PDMS and the Au NS was enlarged, as shown in Fig. 4a and b. The response of the TENG was fast and in sound agreement with the pushing/releasing profile, even for a large pushing force (Figs. S6 and S7). This

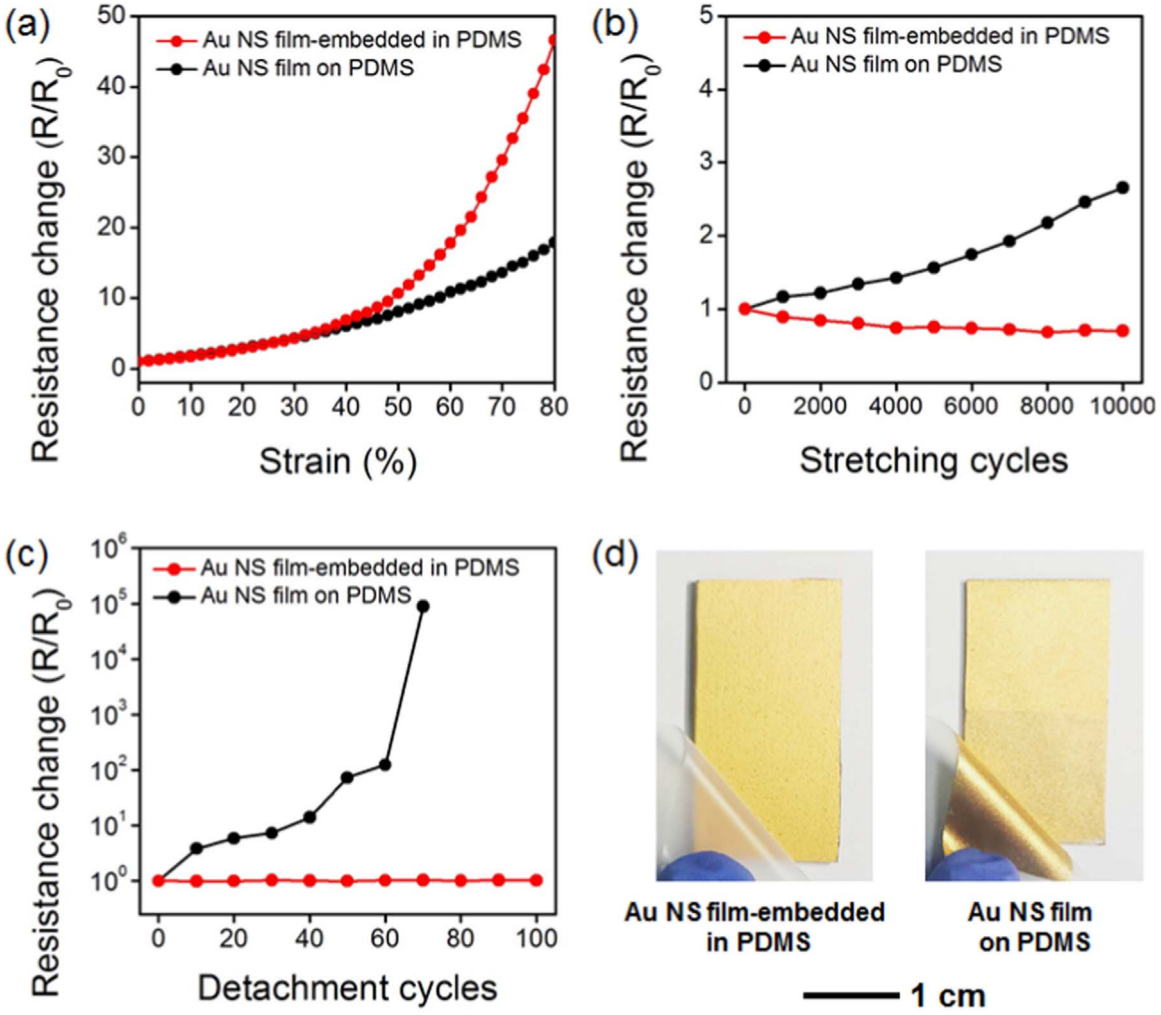

Fig. 2. (a) Change in resistance (R/R_0) for Au NS electrodes in response to tensile strain. (b) Variations of R/R_0 for Au NS electrodes during 10,000 cycles of stretching at a 30% strain. During the cycles, the resistance was measured after the releasing of the strain. (c) Variations of R/R_0 for Au NS electrodes during 100 cycles of the Scotch-tape detachment test. (f) Photographs showing the tape-contact regions of Au NS electrodes after the detachment test.

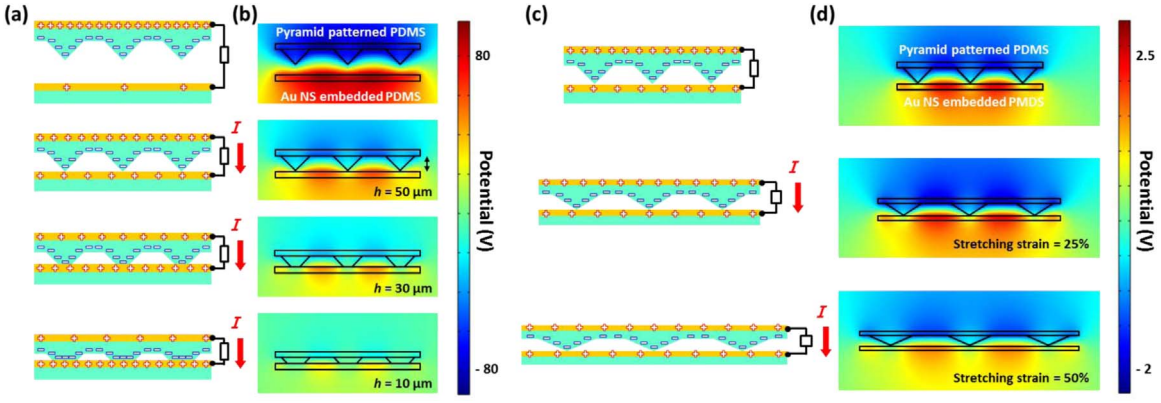

Fig. 3. Schematic illustration of the working mechanism and finite-element simulation of the generated voltage difference of the Au NS-TENG in the (a–b) vertical and (c–d) horizontal motions.

measurement result corresponds to the simulation result in Fig. 3b. After 10,000 cycles with a pushing force of 3 N for the durability test, the output voltage was consistent with the initial output voltage of ~ 60 V (Fig. 4c). Next, we measured the output voltage and current of the Au NS-TENG during the repeated stretching/releasing cycles (Fig. S8). The dependence of the output voltage and current on the stretching strain was also measured from the initial state, where the contact surface between the patterned pyramidal PDMS and the Au NS is not deformed. As the stretching strain was increased from 10% to 50%, the output voltage and current of the Au NS-TENG were increased from 0.1 to 3.1 V and from 7.0 to 90.1 nA, respectively (Fig. 4d and e), because of the closing distance between the two layers for the inducement of a greater electron flow through the circuit. The Au NS-TENG also exhibited a sound responsivity and repeatability, as shown in Figs. S9 and

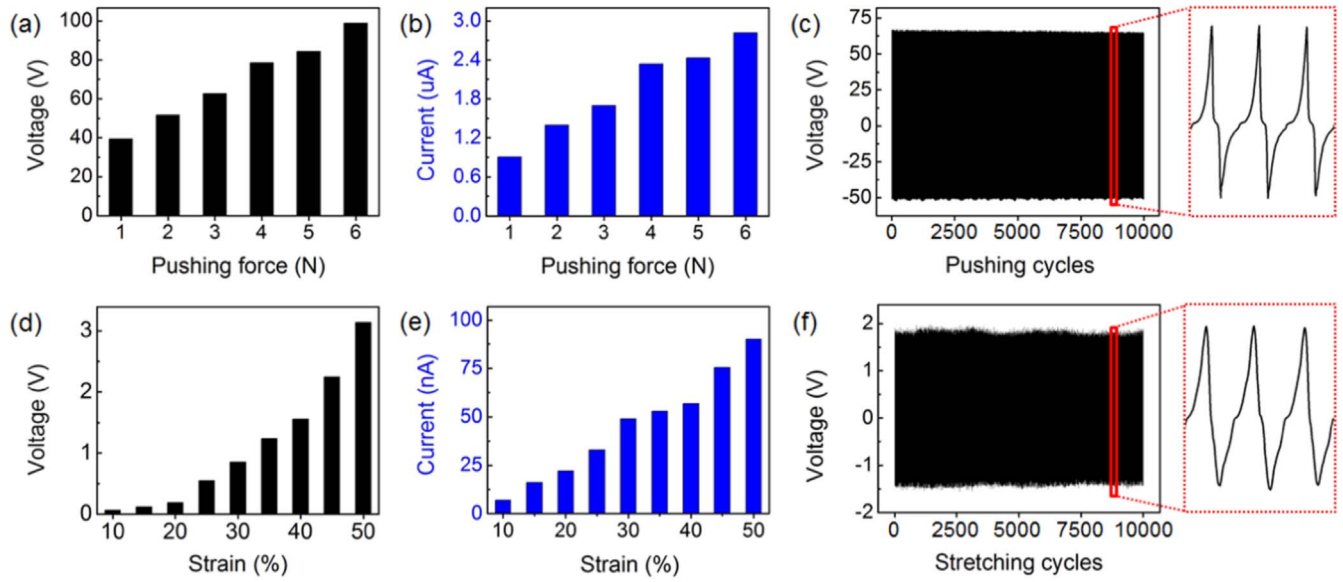

Fig. 4. Output performance of the Au NS-TENG. Voltage output, current output, and durability tests during the 10,000 cycles in the (a–c) pushing mode of the vertical direction and the (d–f) stretching mode of the horizontal direction.

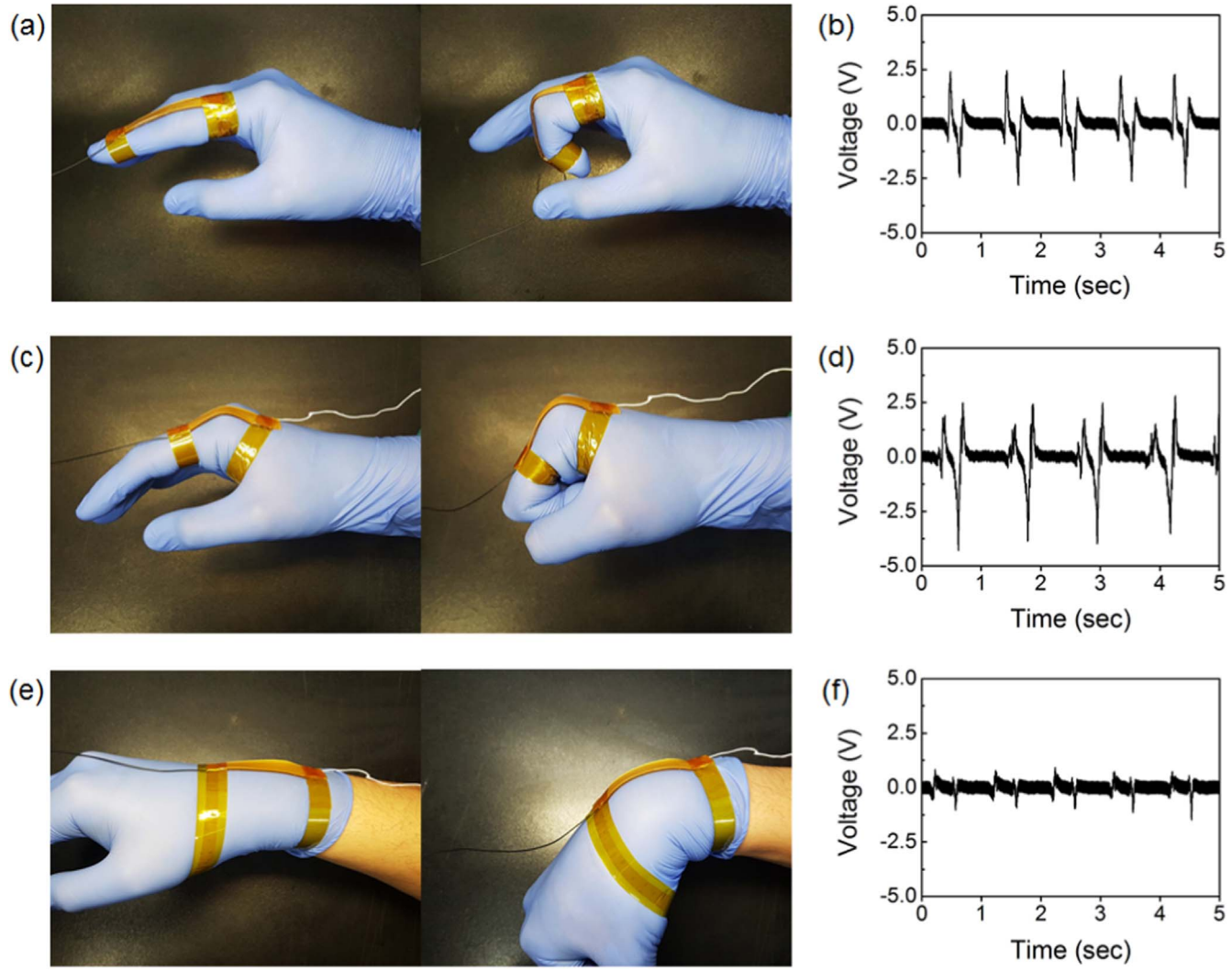

Fig. 5. Photographs and output-voltage responses to the repeated bending/relaxation of the Au NS-TENG that was mounted on the (a, b) index finger, (c, d) knuckle, and (e, f) wrist, respectively.

S10. Over a stretching strain of 50%, the Au NS-TENG cannot be driven properly due to a disconnection between each piece of the Au NS, which is the same reason as that shown in Fig. 2a. Likewise, the stretching-mode durability was tested with 10,000 cycles of the 30% strain and the output voltage was maintained with the initial output voltage of ~ 1.8 V (Fig. 4f). These results show that the fully stretchable and highly durable proposed device can harvest various types of biomechanical energy individually or together, and can be easily applied to e-skin and wearable devices.

Next, we evaluated the suitability of the Au NS-TENG in terms of its operation as a self-powered human-motion detector. In order to investigate the sensing performance of the Au NS-TENG to human motions, we attached the TENG to the moving joints of hand such as index finger, knuckle, and wrist (Fig. 5) and measured signals during repeated bending/relaxation cycles. As shown in the Fig. 5, the Au NS-TENG exhibited a high responsivity and good repeatability to strain variation caused by the joint movements without external power supply. The output signal of the Au-NS TENG increased in the order of wrist, knuckle, and index finger, which is due to the different stretching strains of each joint during bending/relaxation. Distinct signal patterns were generated even for same bending/relaxation motion, which allowed us to distinguish between various joints including index finger, knuckle, and wrist, with just one sensor. These results show that the proposed Au NS-TENG can be used for wearable electronic devices due to its self-powered human-motion detection, and an excellent bendability, stretchability, and repeatability.

4. Conclusions

In summary, a fully stretchable and highly durable TENG that is based on an electrode structure for which an Au NS multilayer film is embedded inside an elastomer PDMS matrix has been developed successfully. Owing to the superior mechanical durability and stretchability of the Au NS-embedded in PDMS, the Au NS-TENG can be stably operated using a repetitive pushing mode (with a compressive force up to 6 N) and a stretching mode (with a strain up to 50%). Furthermore, by applying the Au NS-TENG to various parts of the hand, it has been shown that, given the mechanical deformation in repetitive human motion, it is possible to drive the device stably with both vertical and horizontal movements. Therefore, the human-movement detection can be self-powered without an external power supply, and it is expected that the proposed device can be applied to an energy source of the next-generation wearable electronic devices, such as wireless sensors, temperature imaging, medical diagnostics, and self-powered biomedical applications.

Acknowledgements

This work was supported by a grant from the Center for Advanced Soft Electronics (CASE) under the Global Frontier Research Program (2013M3A6A5073177) by the Ministry of Science, ICT and Future Planning.

Appendix A. Supporting information

Supplementary data associated with this article can be found in the online version at http://dx.doi.org/10.1016/j.nanoen.2017.11.001.

References

[1] F.R. Fan, L. Lin, G. Zhu, W. Wu, R. Zhang, Z.L. Wang, Nano Lett. 12 (2012) 3109–3114.
[2] B.U. Hwang, J.H. Lee, T.Q. Trung, E. Roh, D.I. Kim, S.-W. Kim, N.-E. Lee, ACS Nano 9 (2015) 8801–8810.
[3] D.H. Ho, Q. Sun, S.Y. Kim, J.T. Han, D.H. Kim, J.H. Cho, Adv. Mater. 28 (2016) 2601–2608.
[4] J.H. Park, D.Y. Lee, Y.H. Kim, J.K. Kim, J.H. Lee, J.H. Park, T.W. Lee, J.H. Cho, ACS Appl. Mater. Interfaces 6 (2014) 12380–12387.
[5] Q. Sun, W. Seung, B.J. Kim, S. Seo, S.W. Kim, J.H. Cho, Adv. Mater. 27 (2015) 3411–3417.
[6] G.-H. Lim, N.-E. Lee, B. Lim, J. Mater. Chem. C 4 (2016) 5642–5647.
[7] M. Ha, J. Park, Y. Lee, H. Ko, ACS Nano 9 (2015) 3421–3427.
[8] K.Y. Lee, J. Chun, J.H. Lee, K.N. Kim, N.R. Kang, J.Y. Kim, M.H. Kim, K.S. Shin, M.K. Gupta, J.M. Baik, Adv. Mater. 26 (2014) 5037–5042.
[9] J.H. Park, D.Y. Lee, W. Seung, Q. Sun, S.-W. Kim, J.H. Cho, J. Phys. Chem. C 119 (2015) 7802–7808.
[10] G.T. Hwang, V. Annapureddy, J.H. Han, D.J. Joe, C. Baek, D.Y. Park, D.H. Kim, J.H. Park, C.K. Jeong, K.I. Park, Adv. Energy Mater. 6 (2016) 1600237.
[11] Z. Li, J. Chen, J. Zhou, L. Zheng, K.C. Pradel, X. Fan, H. Guo, Z. Wen, M.-H. Yeh, C. Yu, Nano Energy 22 (2016) 548–557.
[12] J.H. Lee, R. Hinchet, T.Y. Kim, H. Ryu, W. Seung, H.J. Yoon, S.-W. Kim, Adv. Mater. 27 (2015) 5553–5558.
[13] L. Zheng, Z. Lin, G. Cheng, W. Wu, X. Wen, S. Lee, Z.L. Wang, Nano Energy 9 (2014) 291–300.
[14] S. Kim, M.K. Gupta, K.Y. Lee, A. Sohn, T.Y. Kim, K.S. Shin, D. Kim, S.K. Kim, K.H. Lee, H.J. Shin, Adv. Mater. 26 (2014) 3918–3925.
[15] P. Bai, G. Zhu, Z.H. Lin, Q. Jing, J. Chen, G. Zhang, J. Ma, Z.L. Wang, ACS Nano 7 (2013) 3713–3719.
[16] W.S. Jung, M.G. Kang, H.G. Moon, S.H. Baek, S.J. Yoon, Z.L. Wang, S.-W. Kim, C.Y. Kang, Sci. Rep. 5 (2015) 9309.
[17] L. Zheng, G. Cheng, J. Chen, L. Lin, J. Wang, Y. Liu, H. Li, Z.L. Wang, Adv. Energy Mater. 5 (2015) 1501152.
[18] Y. Yang, H. Zhang, Z.H. Lin, Y.S. Zhou, Q. Jing, Y. Su, J. Yang, J. Chen, C. Hu, Z.L. Wang, ACS Nano 7 (2013) 9213–9222.
[19] Y. Su, X. Wen, G. Zhu, J. Yang, J. Chen, P. Bai, Z. Wu, Y. Jiang, Z.L. Wang, Nano Energy 9 (2014) 186–195.
[20] J. Yang, J. Chen, Y. Su, Q. Jing, Z. Li, F. Yi, X. Wen, Z. Wang, Z.L. Wang, Adv. Mater. 27 (2015) 1316–1326.
[21] X. Chen, M. Iwamoto, Z. Shi, L. Zhang, Z.L. Wang, Adv. Funct. Mater. 5 (2015) 739–747.
[22] Q. Jing, G. Zhu, W. Wu, P. Bai, Y. Xie, R.P.S. Han, Z.L. Wang, Nano Energy 10 (2014) 305–312.
[23] G. Zhu, C. Pan, W. Guo, C.-Y. Chen, Y. Zhou, R. Yu, Z.L. Wang, Nano Lett. 12 (2012) 4960–4965.
[24] F.R. Fan, Z.Q. Tian, Z.L. Wang, Nano Energy 1 (2012) 328–334.
[25] S. Wang, L. Lin, Z.L. Wang, Nano Lett. 12 (2012) 6339–6346.
[26] Y. Yang, H. Zhang, J. Chen, Q. Jing, Y.S. Zhou, X. Wen, Z.L. Wang, ACS Nano 7 (2013) 7342–7351.
[27] T. Yamada, Y. Hayamizu, Y. Yamamoto, Y. Yomogida, A. Izadi-Najafabadi, D. Futaba, K. Hata, Nat. Nanotechnol. 6 (2011) 296–301.
[28] N. Lu, C. Lu, S. Yang, J.A. Rogers, Adv. Funct. Mater. 22 (2012) 4044–4050.
[29] L. Persano, C. Dagdeviren, Y. Su, Y. Zhang, S. Girardo, D. Pisignano, Y. Huang, J.A. Rogers, Nat. Commun. 4 (2013) 1633.
[30] G. Schwartz, B. Tee, J. Mei, A. Appleton, D. Kim, H. Wang, Z. Bao, Nat. Commun. 4 (2013) 1859.
[31] E. Roh, B.-U. Hwang, D. Kim, B.-Y. Kim, N.-E. Lee, ACS Nano 9 (2015) 6252–6261.
[32] W. Yeo, Y. Kim, J. Lee, A. Ameen, L. Shi, M. Li, S. Wang, R. Ma, S. Jin, Z. Kang, Y. Huang, J.A. Rogers, Adv. Mater. 25 (2013) 2773–2778.
[33] D.-H. Kim, N. Lu, R. Ma, Y.-S. Kim, R.-H. Kim, S. Wang, J. Wu, S. Won, H. Tao, A. Islam, K. Yu, T.-I. Kim, R. Chowdhury, M. Ying, L. Xu, M. Li, H.-J. Chung, H. Keum, M. McCormick, P. Liu, Y.-W. Zhang, F. Omenetto, Y. Huang, T. Coleman, J.A. Rogers, Science 333 (2011) 838–843.
[34] L. Lin, S. Wang, Y. Xie, Q. Jing, S. Niu, Y. Hu, Z.L. Wang, Nano Lett. 13 (2013) 2916–2923.
[35] X. Wang, S. Niu, Y. Yin, F. Yi, Z. You, Z.L. Wang, Adv. Energy Mater. 5 (2015) 1501467.
[36] J. Chen, G. Zhu, W. Yang, Q. Jing, P. Bai, Y. Yang, T.C. Hou, Z.L. Wang, Adv. Mater. 25 (2013) 6094–6099.
[37] P.K. Yang, L. Lin, F. Yi, X. Li, K.C. Pradel, Y. Zi, C.I. Wu, H. He Jr., Y. Zhang, Z.L. Wang, Adv. Mater. 27 (2015) 3817–3824.
[38] F. Yi, L. Lin, S. Niu, P.K. Yang, Z. Wang, J. Chen, Y. Zhou, Y. Zi, J. Wang, Q. Liao, Y. Zhang, Z.L. Wang, Adv. Funct. Mater. 25 (2015) 3688–3696.
[39] K.N. Kim, J. Chun, J.W. Kim, K.Y. Lee, J.-U. Park, S.-W. Kim, Z.L. Wang, J.M. Baik, ACS Nano 9 (2015) 6394–6400.
[40] G. Moon, G.-H. Lim, J. Song, M. Shin, T. Yu, B. Lim, U. Jeong, Adv. Mater. 25 (2013) 2707–2712.
[41] M. Shin, J. Song, G.-H. Lim, B. Lim, J.-J. Park, U. Jeong, Adv. Mater. 26 (2014) 3706–3711.
[42] G.-H. Lim, K. Ahn, S. Bok, J. Nam, B. Lim, Nanoscale 9 (2017) 8938–8944.
[43] S. Wang, L. Lin, Z.L. Wang, Nano Energy 11 (2015) 436–462.
[44] R. Hinchet, W. Seung, S.-W. Kim, Chem. Sus. Chem. 8 (2015) 2327–2344.
[45] K.-E. Byun, Y. Cho, M. Seol, S. Kim, S.-W. Kim, H.-J. Shin, S. Park, S. Hwang, ACS Appl. Mater. Interfaces 8 (2016) 18519–18525.
[46] G. Song, Y. Kim, S. Yu, M.-O. Kim, S.-H. Park, S.M. Cho, D.B. Velusamy, S.H. Cho, K.L. Kim, J. Kim, E. Kim, C. Park, Chem. Mater. 27 (2015) 4749–4755.
[47] Y. Yu, X. Wang, Extrem. Mech. Lett. 9 (2016) 514–530.
[48] W. Seung, M.K. Gupta, K.Y. Lee, K.-S. Shin, J.-H. Lee, T.Y. Kim, S. Kim, J. Lin, J.H. Kim, S.-W. Kim, ACS Nano 9 (2015) 3501–3509.
[49] J.H. Lee, R. Hinchet, S.K. Kim, S. Kim, S.-W. Kim, Energy Environ. Sci. 8 (2015) 3605–3613.
[50] S. Niu, S. Wang, L. Lin, Y. Liu, Y.S. Zhou, Y. Hu, Z.L. Wang, Energy Environ. Sci. 6 (2013) 3576–3583.
[51] S. Niu, Z.L. Wang, Nano Energy 14 (2015) 161–192.

[52] K.Y. Lee, H.-J. Yoon, T. Jiang, X. Wen, W. Seung, S.-W. Kim, Z.L. Wang, Adv. Energy Mater. 6 (2016) 1502566.

Guh-Hwan Lim is a Ph.D. student under the supervision of Prof. Byungkwon Lim at School of Advanced Materials Science & Engineering, Sungkyunkwan University (SKKU). His research interests include controlled synthesis and assembly of anisotropic metal nanostructures for stretchable electronic devices.

Sung Soo Kwak is a Ph.D. student under the supervision of Prof. Sang-Woo Kim at School of Advanced Materials Science & Engineering in Sungkyunkwan university (SKKU). His research interests are fabrications and characterizations of piezoelectric and triboelectric nanogenerator energy harvesting and their applications in self-powered devices.

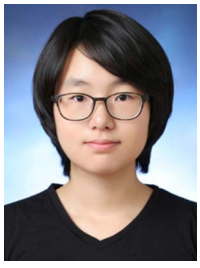

Nayoung Kwon is a Ph.D. student under the supervision of Prof. Byungkwon Lim at School of Advanced Materials Science & Engineering, Sungkyunkwan University (SKKU). Her research interests include the synthesis and self-assembly of metal nanostructures for applications in multi-functional membranes.

Taekyung Kim is a Ph.D. student under the supervision of Prof. Sang-Woo Kim at School of Advanced Materials Science & Engineering in Sungkyunkwan university (SKKU). His research interests include Energy Harvesters.

Han Kim received his Master degree under the supervision of Prof. Sang-Woo Kim at School of Advanced Materials Science & Engineering in Sungkyunkwan university (SKKU). His research interests include Energy Harvesters.

Dr. Seong Min Kim received his Ph.D. degree from University of Cambridge, UK, in 2009. His research interests include multi-physics modeling/simulation, particularly for piezo-phototronic devices and triboelectric nanogenerators.

Dr. Sang-Woo Kim is full professor and SKKU fellow in the School of Advanced Materials Science and Engineering at Sungkyunkwan University (SKKU). He received a Ph.D. in Electronic Science and Engineering from Kyoto University in 2004. After working as a postdoctoral researcher at Kyoto University and University of Cambridge, he spent 4 years as an assistant professor at Kumoh National Institute of Technology. He joined SKKU in 2009. He recently received MCARE 2016 Award (ACerS-KIChE), The Republic of Korea President's Award for Scientific Excellence (2015), National Top 100 Research Award (2015), etc. His recent research interest is focused on piezoelectric/triboelectric nanogenerators, photovoltaics, and 2D materials including graphene, h-BN, and TMDs. He has published over 200 research papers (h-index of 46) and holds over 80 domestic/international patents. Now he is a director of SAMSUNG-SKKU Graphene/2D Research Center and is leading National Research Laboratory for Next Generation Hybrid Energy Harvester. He is currently serving as an Associate Editor of *Nano Energy* (Elsevier) and an Executive Board Member of *Advanced Electronic Materials* (Wiley).

Dr. Byungkwon Lim is Associate Professor in the School of Advanced Materials Science and Engineering at Sungkyunkwan University (SKKU), Korea. He received the Ph.D. degrees in Chemical and Biological Engineering from Seoul National University in 2004. From 2004 to 2007, he worked as a senior researcher at R&D Center of LG Chem, Korea. After working as a postdoctoral researcher at Washington University at St. Louis in USA from 2007 to 2010, he joined SKKU as Assistant Professor in 2010. His recent research interest is focused on synthesis and assembly of nanomaterials for applications in energy storage & generation, and soft electronics.